Iron carbonate formation kinetics onto corroding and pre-filmed carbon steel surfaces in carbon dioxide corrosion environments

R. Barker,[1a)] I. Al Shaaili,[1] R. A. De Motte,[1] D. Burkle,[1] T. Charpentier[1] S. M. Vargas,[2] and A. Neville,[1]

[1]Institue of Functional Surfaces, University of Leeds, Leeds, LS2 9JT, United Kingdom
[2]BP America, Inc., Houston, Texas 77079

[a)] Corresponding Author – R.J.Barker@leeds.ac.uk

Abstract

This work investigates the Corrosion Layer Accumulation Rate (CLAR) of iron carbonate ($FeCO_3$) onto X65 carbon steel in carbon dioxide containing environments using the direct method of corrosion layer mass gain measurement. Glass cell experiments were performed at 80°C and pH 6.3 or 6.8 over a range of bulk $FeCO_3$ saturation ratios using both actively corroding carbon steel and steel pre-filmed with $FeCO_3$. The CLARs obtained from experiments using actively corroding samples displayed strong agreement with the most recently developed precipitation model by Sun and Nesic at high supersaturation for pH 6.3 and 6.8, but a disparity at low supersaturation for the solution at pH 6.8. The observed discrepancy was attributed to the significant difference in surface saturation ratio between the two conditions when the steel is actively corroding. CLARs determined for pre-$FeCO_3$ filmed carbon steel show that the kinetics of $FeCO_3$ formation reduce significantly once the film establishes a protective barrier at lower values of supersaturation. The results highlight the contrast between surface layer accumulation kinetics in the early stages of growth and those encountered in the long-term after the development of a protective film.

Key words: CO_2 corrosion, iron carbonate, carbon steel, corrosion product kinetics, corrosion layer accumulation rate.

1. Introduction

In CO_2 environments encountered during oil and gas production and transportation the formation of iron carbonate ($FeCO_3$) corrosion products on the internal walls of carbon steel is a common occurrence. The development of this corrosion product can have a

significant effect on the dissolution behaviour of the underlying steel[1]. The layer produced is able to reduce corrosion rates by over an order of magnitude in some instances. The ability of $FeCO_3$ to achieve such a dramatic reduction in corrosion rate is believed to be achieved through a surface blocking effect as a result of the crystals being in direct contact with the steel substrate. However, it has also been suggested that the layer acts as a diffusion barrier to electrochemically active species involved in the cathodic reactions[2, 3].

Understanding the degree of protection afforded by the layer and its associated kinetics of formation is of interest to corrosion engineers when developing a corrosion management strategy. $FeCO_3$ precipitation is achieved when the product of the concentrations of Fe^{2+} (iron ions) and CO_3^{2-} (carbonate ions) exceed the solubility limit, resulting in the following reaction:

$$Fe^{2+}_{(aq)} + CO^{2-}_{3\,(aq)} \rightarrow FeCO_{3\,(s)} \quad (1)$$

The rate of development of $FeCO_3$, as well as the morphology and level of protection are strongly associated with the kinetics of this reaction[3]. It has been suggested that although crystallisation consists of a nucleation and growth phase, in the case of heterogeneous crystallisation, the overall kinetics are believed to be dominated by crystal growth[3]. However, though this may be true for cases in which the solution is highly super-saturated with $FeCO_3$ (where induction times are rapid), this process could be different in a scenario whereby the level of saturation is very low at the steel surface and the induction time is prolonged, as may be the case in certain oil and gas operating scenarios.

The driving force for precipitation of $FeCO_3$ is the supersaturation or saturation ratio (S) of $FeCO_3$. Supersaturation is defined as:

$$S = \frac{[Fe^{2+}][CO_3^{2-}]}{K_{sp}} \quad (2)$$

where

$$K_{sp} = [Fe^{2+}]_{eq}[CO_3^{2-}]_{eq} \quad (3)$$

where $[Fe^{2+}]$ and $[CO_3^{2-}]$ (in mol/dm^3) are the ferrous and carbonate ions concentrations, respectively and K_{sp} (in mol^2/dm^6) is the solubility product for $FeCO_3$. $[Fe^{2+}]_{eq}$ and $[CO_3^{2-}]_{eq}$ are the equilibria concentrations of the ferrous and carbonate species. It is worth noting that typically, activities of species are used in Equation (2) as opposed to specie concentration. However, the concentration of Fe^{2+} and CO_3^{2-} can be used when the effect of ionic strength is integrated into K_{sp} models.

Dugstad[4] suggested that a 'high degree' of supersaturation is necessary in the bulk solution to obtain appreciable levels of $FeCO_3$ formation on the steel surface. However, more recent studies have indicated that enough surface deposition to provide suppression of carbon steel corrosion rates can occur in systems with a bulk saturation below 2 [2, 5-7].

In principle, there exist two steps involved in the precipitation processes; nucleation and particle growth. Theoretically, two scenarios can be encountered for $FeCO_3$ precipitation; either nucleation followed by growth, or nucleation followed by nucleation and growth. In previous research, different laboratory-based techniques have been implemented to determine $FeCO_3$ precipitation/accumulation kinetics, ranging from measuring the dissolved ferrous ion concentration change in the bulk solution (such as in the work by van Hunnik et al.[8]) to evaluating the growth of $FeCO_3$ onto well characterised seed crystals (as in the work by Johnson and Tomson and Greenberg and Tomson[9-11]), to a more recent study by Sun and Nesic[3] involving direct corrosion layer mass gain measurements.

Each of the aforementioned authors have proposed their own semi-empirical expressions for the kinetics of $FeCO_3$ formation as a function of supersaturation and temperature. However, arguably the most accurate model developed to date is the corrosion layer accumulation rate (CLAR) model proposed by Sun and Nesic[3]. In their research, Sun and Nesic showed that the most reliable technique for determining the kinetics of $FeCO_3$ formation onto steel substrates was the direct method of corrosion layer mass-change measurement. They also highlighted that the approach of previous experimental methodologies adopted by other authors meant they could not be applied to corroding steel surfaces, and/or greatly over-estimated the level of $FeCO_3$ deposition onto the substrate. Sun and Nesic also made the distinction between the precipitation rate and the CLAR, identifying that not all $FeCO_3$ which precipitates in the system ends up on the steel

surface. This is a concept that will be discussed later, but it is important to make the distinction here that from this point in the paper onwards, precipitation rate (PR) will refer to precipitation as a whole (i.e. the rate of $FeCO_3$ formation in the whole system; in the bulk solution and at surface) while CLAR refers to the rate of formation exclusively on the corroding or pre-filmed steel surface (which is the main focus of interest from an oil and gas industry perspective).

Perhaps most importantly within the work by Sun and Nesic[3], the importance of local supersaturation at the corroding steel surface was discussed, along with the role this may play in influencing the CLAR characteristics. By considering $FeCO_3$ nucleation and growth onto a corroding steel sample as well as a non-corroding stainless steel sample as a function of different bulk values of supersaturation, they were able to show that the CLAR of $FeCO_3$ is not exclusively controlled by the bulk solution chemistry, and that surface concentration of species is important for actively corroding surfaces (a concept eluded to by van Hunnik et al.[8] during the development of their model). Experiments performed at a supersaturation of 60 at 80^{o}C and pH 6.6 produced no nucleation and growth of $FeCO_3$ on stainless steel, whereas a substantial film developed on mild steel under the same operating conditions. However, it must be noted that the two surfaces of are not entirely comparable with one another i.e. stainless steel is not entirely analogous to non-corroding carbon steel surface. Nonetheless, they raise an interesting point of discussion.

Currently, all $FeCO_3$ precipitation models (or CLAR models, depending on the authors and their adopted methodologies) available within literature are expressed as a function of bulk supersaturation, not the local conditions/ supersaturation at the steel surface. From the perspective of accurately modelling such a process, this makes little sense. Although the bulk supersaturation is undoubtedly important in the film formation process, Fe^{2+} is produced at the surface of a corroding carbon steel sample, while H^{+} ions are consumed on the steel surface (or the iron carbide (Fe_3C) layer is this is present). The corrosion of carbon steel results in a higher pH at the steel-electrolyte interface, with this behaviour being confirmed both computationally[12, 13] through numerical simulation and experimentally via the use of a mesh capped pH electrode positioned in the near–surface region[14]. The high local pH increases CO_3^{2-} concentration at the surface[13], meaning less Fe^{2+} ions are required to locally exceed the solubility limit of $FeCO_3$.

Considering that the steel is corroding, the concentration of Fe^{2+} is greater at the surface compared to the bulk solution. This effect, coupled with the higher local CO_3^{2-} concentration results in increased supersaturation at the steel-electrolyte interface. It is therefore theoretically possible to achieve $FeCO_3$ formation locally at the steel surface in a solution when the bulk solution is under-saturated. Considering this notion, determining the bulk solution chemistry along with surface corrosion rates/ reactions is critical to understanding and predicting the rate of $FeCO_3$ formation. It is also important to understand the nucleation and growth kinetics of $FeCO_3$ throughout the whole lifecycle of a corroding surface. This includes from when the surface is clean, when there is a build-up of a layer and when a well-established and protective film exists.

In this paper, the CLAR of $FeCO_3$ is characterised on both an actively corroding surface (i.e. during the early stages of corrosion product growth where there is a flux of Fe^{2+} ions from the surface) and onto a well-established, protective $FeCO_3$ film (i.e. representing the long-term growth rate when the production of Fe^{2+} from the surface is significantly reduced by film formation). The latter approach is a technique which has not been conducted before within literature. The purpose of the work is to establish how $FeCO_3$ kinetics shift as the film transitions from actively corroding to a system where there is minimal corrosion as a result of full coverage of a protective film. The study here is conducted under static conditions with slight agitation of the test solution using a magnetic stirrer to enable fair comparison with the previously generated prediction model of Sun and Nesic[3] under similar hydrodynamic conditions. It is also important to stress here that these observations are applicable to environments where no corrosion inhibitor is administered to the system.

2. Experimental Procedures

All experiments were performed in a glass cell as shown in the schematic in Figure 1.

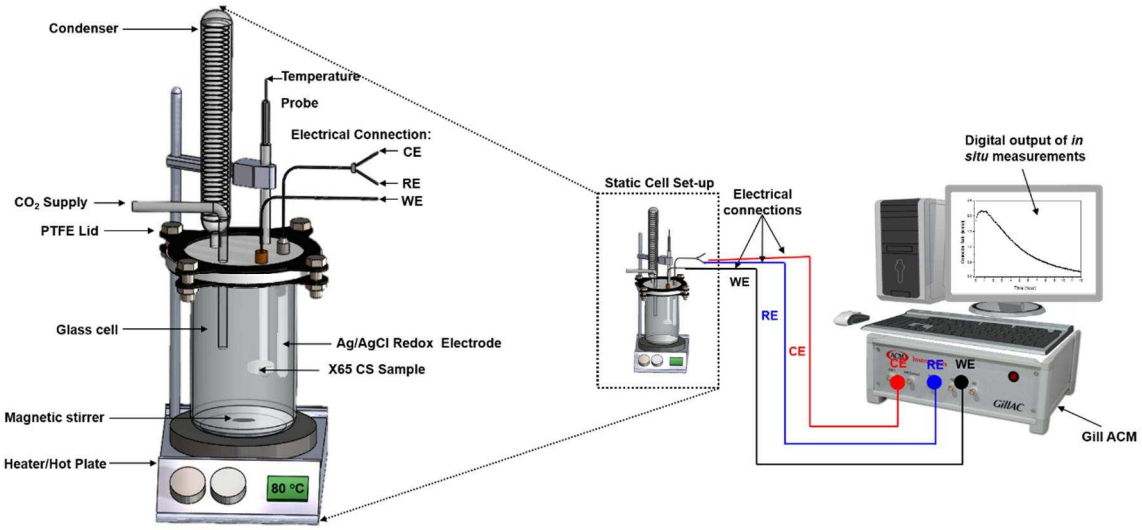

Figure 1: Schematic of test cell for CLAR and electrochemical experiments

A CO_2-saturated 3.5 wt.% NaCl solution was used in all experiments which was agitated through the use of a magnetic stirrer set at 250 rpm. The pH was controlled in each experiment at either 6.3 or 6.8 through the addition of sodium hydrogen bicarbonate ($NaHCO_3$) and CO_2 was bubbled into the solution for 12 hours before the experiment to deoxygenate the solution. CO_2 was also bubbled into the test vessel during the entire test to maintain saturation. Two main types of experiments were performed. These consisted of either 20 h experiments to nucleate and grow reproducible and protective $FeCO_3$ films on the X65 steel surface, or short duration (2 hours) experiments to evaluate $FeCO_3$ CLARs at different levels of initial bulk supersaturation (ranging from 0 to 200). In all experiments the surface area to volume ratio was maintained at 4.9 cm^2 per 1L of electrolyte. The X65 carbon steel samples were all cut from a 25 mm diameter stock bar which possessed a ferritic-pearlitic microstructure as shown in Figure 2. The composition of the steel is also provided in Table 1. The methodologies adopted for each of the two experimental stages are outlined in the following sections.

2.1 20 hours film growth experiments

The overall aim of the research was to compare and contrast the CLAR of $FeCO_3$ onto a freshly ground, actively corroding steel and a steel surface pre-filmed with $FeCO_3$ to simulate early and late kinetics during the film formation process. To achieve the latter, it was necessary to generate protective $FeCO_3$ films on a steel surface which had a reproducible mass. For these experiments, wet-ground X65 steel samples were inserted

into a CO_2-saturated 3.5 wt.% NaCl brine at 80°C and pH 6.8. Prior to immersion in the test solution, the samples were wet-ground with 600-grit silicon carbide (SiC) paper, rinsed with ethanol and degreased with acetone. No initial addition of Fe^{2+} ions was performed at the start of these experiment and exposure of the steel sample to the test solution for 20 h ensured the formation of a protective $FeCO_3$ film.

To determine the $FeCO_3$ mass at the end of the 20 h experiment, the mass gain technique was implemented. This was conducted by recording the mass of the coupon directly after the experiment with and without the presence of the $FeCO_3$ layer. The $FeCO_3$ corrosion product was removed using Clarke's solution (prepared by combining 20g antimony trioxide (Sb_2O_3) and 50 g stannous chloride ($SnCl_2$) with 1L hydrochloric acid (HCl) at room temperature) and the difference between the two recorded masses provided the mass of $FeCO_3$ on the steel surface.

Electrochemical measurements were also performed on the steel samples to determine in situ corrosion rates. Wires were soldered to the back of each sample before embedding in a non-conducting resin. Again, the exposed area of the sample was 4.9 cm^2. The in-situ corrosion rate was followed using the linear polarisation resistance technique with a conventional three-electrode cell consisting of the steel sample, a Ag/AgCl reference electrode and a platinum counter electrode. The steel sample was polarised ±15 mV about the open circuit potential (OCP) at a scan rate of 0.25 mV/s every 10 minutes to produce a polarisation resistance which was subsequently corrected for solution resistance (determined using Electrochemical Impedance Spectroscopy) to produce a charge-transfer resistance (R_{ct}). This value was then converted into a corrosion rate using the Stern-Geary relationship (Equation (4))

$$i_{corr} = \frac{B}{R_{ct}} = \frac{1}{R_{ct}} \frac{\beta_a \beta_c}{2.303(\beta_a + \beta_c)} \quad (4)$$

where B is the Stern-Geary coefficient, β_a is the magnitude of the anodic Tafel constant and β_c is the magnitude of the cathodic Tafel constant. The value of i_{corr} was then used in conjunction with Faraday's Law and an appropriate conversion factor (Equation (5)) to obtain the corrosion kinetics in mm/year over the 20 h experiment.

$$CR = \frac{Ki_{corr}M_{Fe}}{nF\rho} \quad (5)$$

where K is a conversion factor to obtain corrosion rate (CR) in units of mm/ year (K = $3.16x10^5$), M_{Fe} is the molar mass of iron (55.8 g), n is the number of electrons freed in the corrosion reaction (2 electrons), ρ is the density of steel (7.87 g/ cm^3) and F is the Faraday constant (96,485 coulomb/ mole)

Tafel polarisation measurements were performed to determine the effect of the $FeCO_3$ film on the anodic and cathodic reactions and enable appropriate values to be used for β_a and β_c in the Stern-Geary relationship. These experiments were conducted at 2 hours and 20 h and were not used for subsequent experiments as the polarisation may have induced changes in the morphology and/ or quantity of $FeCO_3$ accumulated on the steel surface. At the end of the 2 hours or 20 h test, either an anodic scan or cathodic scan was performed by polarising from OCP to +150 or -400 mV, respectively.

2.2 2 hours CLAR experiments onto wet-ground ground and pre-filmed samples

Short term experiments over 2 hours were conducted to establish CLARs as a function of bulk supersaturation. This consisted of inserting either wet-ground steel or pre-filmed samples into a CO_2-saturated 3.5 wt.% NaCl 80°C solution at either pH 6.3 or 6.8. In these experiments an initial supersaturation of between 0 and 200 was established through the addition of Fe^{2+} ions in the form of a deoxygenated ferrous chloride solution ($FeCl_2 \cdot 4H_2O$). After 2 hours exposure of the sample to the test solution, the total mass of $FeCO_3$ on the steel surface was obtained using the mass gain technique previously discussed. In the case of the pre-filmed samples, the estimated, average repeatable mass recorded in the first stage of the test was subtracted from the total mass measured in these experiments to produce a mass gain over the 2 hours test only. This enabled the CLAR onto the pre-filmed sample to be established and compared with CLARs onto the corroding, wet-ground steel surface. Further details of the mass gain methodology and the equations implemented can be found in publications by Sun and Nesic[3] and de Motte et al.[15].

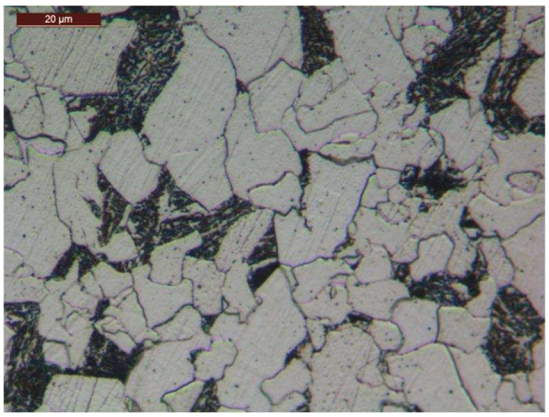

Figure 2: Microstructure of API 5L X65 depicting a ferritic-pearlitic structure; Surface preparation consisted of polishing the surface using 3 µm diamond suspension to attain a mirror finish, followed by etching in a 2% nital solution for 10 to 20 seconds

Table 1: Elemental composition (wt.%) of API 5L X65 carbon steel

C	Si	Mn	P	S	Cr	Mo	Fe
0.12	0.18	1.27	0.008	0.002	0.11	0.17	Balance

3. Results and Discussion

3.1 CLAR onto a wet-ground steel surface

The initial tests performed considered CLAR onto wet-ground, corroding X65 carbon steel surfaces at pH 6.3 and pH 6.8 at 80°C over a range of supersaturation values from ~0 to 200. The Fe^{2+} concentration required for each desired initial saturation value was determined using Equation (2). According to the bulk equilibrium calculations based on the CO_2-H_2O system at 80°C[15], the CO_3^{2-} ion concentration can be calculated to be 7.70 × 10^{-5} mol·dm^{-3} for pH 6.8 and 7.70 × 10^{-6} mol·dm^{-3} for pH 6.3. The value of K_{sp} was determined to be 1.58 × 10^{-5} mol^2dm^{-6} using the model proposed by Sun and Nesic which is a function of temperature as well as ionic strength as shown in Equation (6).

$$\log K_{sp} = -59.3498 - 0.041377T_k - \frac{2.1963}{T_K} + 24.5724\log_{10}(T_K) + 2.518I^{0.5} - 0.657I \quad (6)$$

The level of supersaturation was determined at the very beginning and the end of each mass gain experiment using spectrophotometry. The arithmetic mean of these values and their total range were used to establish correlations with the recorded CLARs.

The first set of experiments conducted using actively corroding steel were performed without the initial addition of Fe^{2+} ions at pH 6.3 and 6.8. Figure 3 shows SEM images of the X65 carbon steel samples exposed to each pH at 80°C after 2 hours. At the end of each experiment, the bulk supersaturation was recorded at ~0.5 and ~1.5 for pH 6.3 and 6.8, respectively. The images indicate that accumulation of $FeCO_3$ occurs on the steel surface in the static system at very low levels of bulk supersaturation, and even when bulk supersaturation is less than 1 in the case of pH 6.3. These initial observations already suggests surface concentration is important in the context of $FeCO_3$ surface accumulation as the bulk conditions are not thermodynamically favourable for nucleation and growth of $FeCO_3$ at pH 6.3, yet $FeCO_3$ crystals were visible on the steel surface.

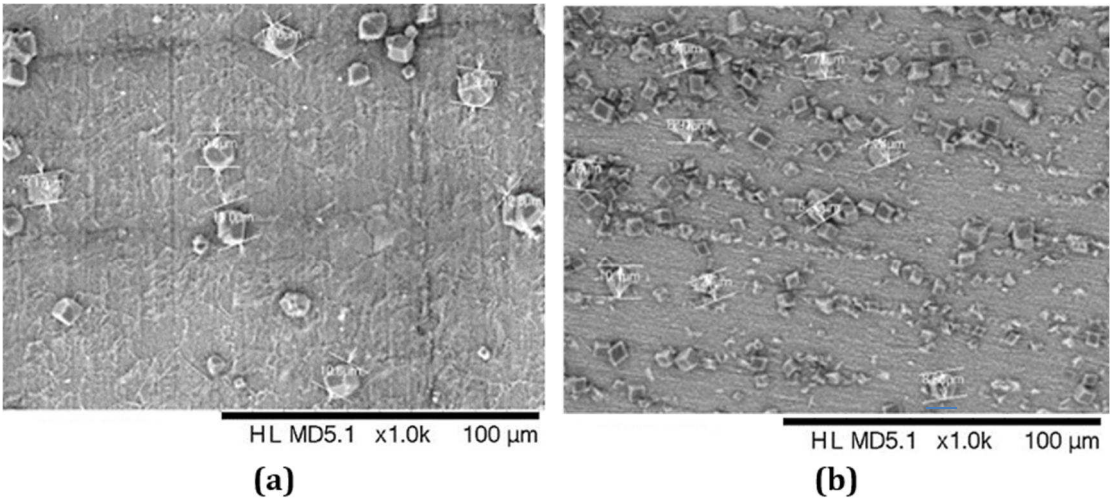

Figure 3: SEM images of wet-ground X65 carbon steel samples after exposure for 2 hours in a 3.5 wt.% NaCl CO_2-saturated solution at 80°C with an initial supersaturation (S) of 0 at (a) pH 6.3 and (b) pH 6.8

Figure 4 shows the SEM images of the wet-ground steel surfaces when exposed to solutions with an initial bulk supersaturation of 50, 100 and 150 at pH 6.8 and 80°C for 2 hours at pH 6.8. Increasing the bulk supersaturation clearly increases the CLAR of $FeCO_3$, demonstrating that the bulk supersaturation influences the formation of the corrosion product. What becomes evident from analysis of the SEM images is that as bulk

supersaturation increases, the number of crystals increases and the average crystal diameter decreases. This can be explained by considering the relationship between crystal nucleation and growth processes and supersaturation. Nucleation rate is known to increase exponentially with supersaturation, whilst growth varies linearly[16]. Consequently, as supersaturation rises, there is a significant increase in nucleation rate (more so than that associated with crystal growth) which results in the development of numerous, smaller crystals as a greater proportion of the Fe^{2+} ions contribute towards nucleation as opposed to growth. Furthermore, confirmation that the crystals developed on the steel surface are indeed $FeCO_3$ is provided by the XRD patterns shown in Figure 5.

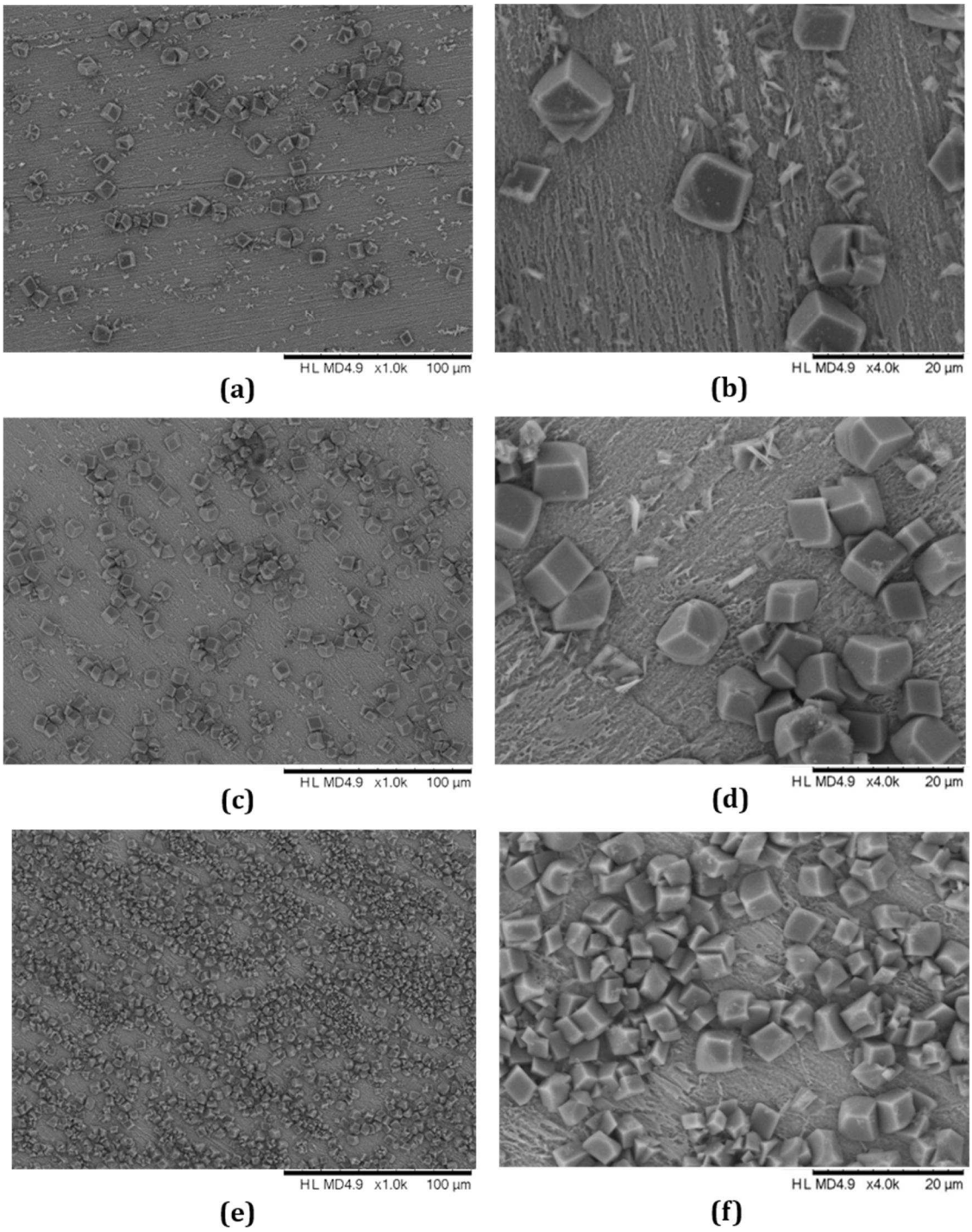

Figure 4: SEM images of wet-ground X65 carbon steel samples after exposure for 2 hours in a 3.5 wt.% NaCl CO_2-saturated solution at pH 6.8 and 80°C with an initial supersaturation (S) of (a)/ (b) $S = 50$, (c)/ (d) $S = 100$, (e)/ (f) $S = 150$.

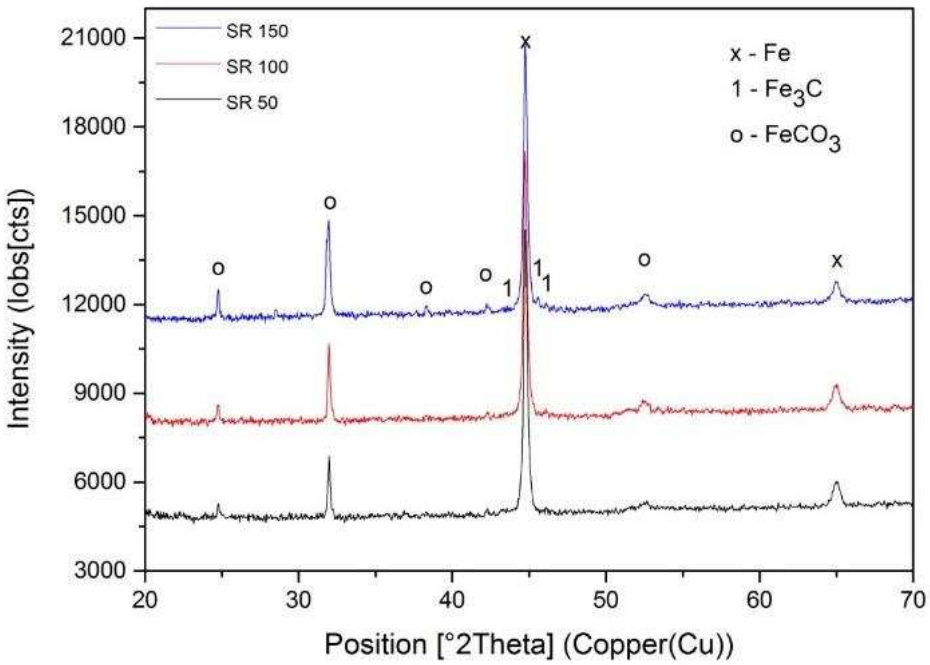

Figure 5: XRD patterns of wet-ground X65 carbon steel samples after exposure for 2 hours in a 3.5 wt.% NaCl CO_2-saturated solution at pH 6.8 and 80°C with initial supersaturation (S) of 50, 100 and 150.

3.2 CLARs onto wet-ground surface and comparison with existing models

Mass gain measurements were conducted on wet-ground samples at pH 6.3 and 6.8 across a range of initial supersaturation values from 0 to 200. The CLARs determined over the first 2 hours of exposure are plotted in Figure 6 against the average of the initial and final bulk supersaturation in each experiment determined using the Fe^{2+} concentration measured with the aid of spectrophotometry. Figure 6(a) shows the variation in bulk supersaturation over the test duration using horizontal error bars and compares the CLARs measured here with two of the existing semi-empirical models from literature, whilst Figure 6(b) shows the CLARs in the absence of horizontal error bars and other models for the purpose of clarity.

Four semi-empirical growth rate expressions for $FeCO_3$ precipitation exist in literature which take the form shown in Equation (7).

$$P_{FeCO_3} = k_r \frac{A}{V} \sigma^r \quad (7)$$

where k_r is a kinetic constant (in the form of a temperature dependent Arrhenius function), A/V is the ratio of surface area (of seed crystals or steel sample) to solution

volume, σ is the driving force and r is the reaction order. The four models in question have been developed by Greenberg and Tomson[9, 10], Johnson and Tomson[11], van Hunnik et al.[8] and Sun and Nesic[3]. Table 2 provides a detailed description of each of the four models which is extracted from a review paper by Barker et al.[17]. It must be stressed that all models predict precipitation rates in $mol \cdot m^{-3} s^{-1}$.

To summarise each model's development, the methods employed by both Greenberg and Tomson[9, 10] and Johnson and Tomson[11] involve the estimation of precipitation rate through the measurement of the change in Fe^{2+} concentration in the bulk solution. The systems considered by both sets of authors involved low levels of supersaturation where the growth was evaluated on well characterised seed crystals suspended in a bulk solution.

The method of van Hunnik et al.[8] also relied upon the measurement of Fe^{2+} concentration. However, these experiments determined the initial deviation of Fe^{2+} concentration increase once the system passed through the pH corresponding to the solubility of $FeCO_3$. The tests by van Hunnik et al.[8] used a corroding steel pipe surface as the substrate.

The experimental technique implemented by Sun and Nesic[3] invoked the direct measurement technique to determine $FeCO_3$ accumulation onto a corroding carbon steel surface. This was achieved by measuring the mass gain of a $FeCO_3$ covered sample (the same technique adopted in this work). Steel samples were placed in a deoxygenated NaCl solution and ferrous chloride was added to create specific levels of $FeCO_3$ saturation. After removal, samples were dried and weighed, followed by removal of the corrosion product layer using Clarke's solution before being weighed again. The difference in mass was then used along with the exposure time to determine a CLAR, (which could also be expressed as a precipitation rate), as shown in Table 2.

Table 2: A summary and comparison of the four available $FeCO_3$ precipitation models available in literature – adapted from Barker et al.[17]

	Greenberg and Tomson	Johnson and Tomson	Van Hunnik, Pots and Hendriksen	Sun and Nesic
Summary	Crystals were pre-grown in an anoxic environment and washed to remove counter-ions. Consequently, well characterised seed crystals were used as a substrate. Precipitation kinetics were determined by using the traditional (indirect) technique which involves measuring Fe^{2+} concentration change. Precipitation was initiated by raising pH by lowering the CO_2 partial pressure in the system.	Crystals were pre-grown in an anoxic environment and washed to remove counter-ions. Consequently, well characterised seed crystals were used as a substrate. Precipitation kinetics were determined by using the traditional (indirect) technique which involves measuring Fe^{2+} concentration change. Equilibrium was established over 48 hours, then temperature was ramped, with samples being removed from the reaction vessel every 30 mins.	Experiments were performed in a flow loop under anoxic conditions. Precipitation kinetics were determined by using the traditional (indirect) technique which involves measuring Fe^{2+} concentration change. The rate was determined from the initial deviation from the linear increase of the Fe^{2+} concentration after the saturation point was exceeded.	Experiments were performed in a glass cell. Steel samples were placed in a deoxygenated saline solution. Ferrous chloride was added to create a specific level of $FeCO_3$ saturation. Samples were removed at regular intervals. Precipitation rate was determined by measuring the mass difference with and without the $FeCO_3$ layer.
Substrate	$FeCO_3$ seed crystals	$FeCO_3$ seed crystals	Steel pipe surface	Steel coupons
Solution	Deoxygenated water	Deoxygenated water	Deoxygenated 1 wt.% NaCl solution	Deoxygenated 1 wt.% NaCl solution
Precipitation rate (P_{FeCO_3}) (mol/ m³/ s)	$e^{A_0-\frac{E}{RT}}\frac{A}{V}K_{sp}\left[\sqrt{S}-1\right]^2$	$e^{A_0-\frac{E}{RT}}\frac{A}{V}K_{sp}\left[\sqrt{S}-1\right]^2$	$e^{A_0-\frac{E}{RT}}\frac{A}{V}K_{sp}(S-1)\left(1-\frac{1}{S}\right)$	$e^{A_0-\frac{E}{RT}}\frac{A}{V}K_{sp}(S-1)$
Solubility product, K_{sp} (mol²dm⁶)	$log(K_{sp}) = -59.2385 - 0.041377(T_K) - \frac{2.1963}{T_K} + 24.5724log(T_K)$	$log(K_{sp}) = -0.4343\left(\frac{-30140}{8.314(T_K)} + 36.22\right)$	No K_{sp} value identified, therefore Sun and Nesic K_{sp} value used in calculations as this is the most recent model proposed in literature	$log(K_{sp}) = -59.3498 - 0.041377(T_K) - \frac{2.1963}{T_K} + 24.5724log(T_K) + 2.518(I^{0.5}) - 0.657(I)$
Constant, A_0	44.4	56.3	52.4	28.2
Activation Energy, E (kJ/ mol)	95.8	127.3	119.8	64.9
Area, A	Area of crystals surfaces	Area of crystal surfaces	It is not clear from the paper whether the area used was determined from crystal size or from the area of the corroding electrode	Area refers to that of the corroding sample
Volume, V	Volume of solution	Volume of solution	Volume of solution	Volume of solution

Figure 6(a) shows the CLARs determined at pH 6.3 and 6.8 in comparison to the van Hunnik et al. and Sun and Nesic models which have been adapted to produce units of $mol \cdot m^{-2}s^{-1}$. As stated previously, the Greenberg and Tomson, as well as the Johnson and Tomson precipitation models are both determined by evaluating the growth of $FeCO_3$ onto well characterised seed crystals and previous work by Sun and Nesic identified that these models should not be used as they consider homogeneous precipitation with no steel substrate involved. It is also important to note that neither Greenberg and Tomson nor Johnson and Tomson explicitly stated in their publications that these kinetic expressions can or should be applied to a corroding steel surface in a CO_2 environment. With this in mind, both the Greenberg and Tomson and Johnson and Tomson models have been excluded from this comparison.

In terms of the van Hunnik et al. model, this expression can be used to determine the CLAR. Again, the precipitation rate determined by this model in Table 2 is expressed in $mol \cdot m^{-3}s^{-1}$. However, Gulbrandsen[18] indicated that the van Hunnik model can be rearranged to produce a precipitation rate per unit area ($mol \cdot m^{-2}s^{-1}$):

$$\frac{V}{A} P_{FeCO_3} = A_p e^{\frac{E}{RT}} K_{sp} (S-1) \left(1 - \frac{1}{S}\right) \quad (8)$$

Nonetheless, this expression still assumes that all precipitated $FeCO_3$ in the system ends up accumulating on the steel surface, a notion which is known to be untrue. This relates back to the fact that a distinction needs to be made between the precipitation rate (i.e. total formation of $FeCO_3$) and the CLAR (i.e. relating to the quantity of $FeCO_3$ on a steel surface). This distinction has been made by Sun and Nesic, and in light of this observation, Sun and Nesic [44] proposed a new semi-empirical expression for the CLAR, founded on their direct mass-change results:

$$CLAR = e^{A_0 - \frac{E}{RT}} K_{sp} (S-1) \quad (9)$$

where CLAR is the corrosion layer accumulation rate in $mol \cdot m^{-2}s^{-1}$. This equation takes the same form and uses the same constants as that developed by Sun and Nesic in Table 2. However, the A/V ratio is omitted from this equation to make it applicable to a corroding steel surface. If all Fe^{2+} ions that precipitate from the solution end up on the steel surface, then the precipitation rate (P_{FeCO3}) is equal to the CLAR corrected for the A/V ratio:

$$P_{FeCO_3} = \frac{A}{V}\, CLAR \tag{10}$$

Using the two rearranged expressions developed by van Hunnik et al. and Sun and Nesic, the two CLAR models are compared against the collected data in Figure 6(a). Unfortunately, it was not clear in the publication by van Hunnik et al. as to which correlation was used for K_{sp}. Therefore, the correlation by Sun and Nesic in Equation (6) was used, both with and without the ionic strength expression to highlight the sensitivity of the model. For the Sun and Nesic CLAR model, the corresponding K_{sp} model in Table 2 was used.

Referring to Figure 6(a), all models demonstrate an increase in CLAR with supersaturation (as expected), but the predictions span well over two orders of magnitude. In the case of the van Hunnik model[8], although experiments were performed on a corroding steel pipe, the implementation of the Fe^{2+} concentration measurement implicitly assumes that the entire amount of Fe^{2+} lost in the solution is associated with $FeCO_3$ deposition onto the steel surface, something which was demonstrated to be untrue by Sun and Nesic[3] as $FeCO_3$ is also able to precipitate out into the bulk solution as well as onto the steel surface. Consequently, the model of van Hunnik et al.[8] results in an over-estimation of $FeCO_3$ precipitation rate at high saturation levels, regardless of the solubility product implemented.

For experiments performed at pH 6.3 across all supersaturation values and at pH 6.8 at high supersaturation, strong agreement is obtained with the CLARs determined by the Sun and Nesic model[3]. This model was founded based on experimental data gathered using the weight gain method in an identical process to that conducted in this research. Sun and Nesic showed conclusively that the implementation of the weight gain technique, although more cumbersome, offers a more realistic interpretation of the deposition rate onto a corroding steel surface. However, the model developed does not correlate as strongly at low supersaturation with the experiments performed in this work at pH 6.8.

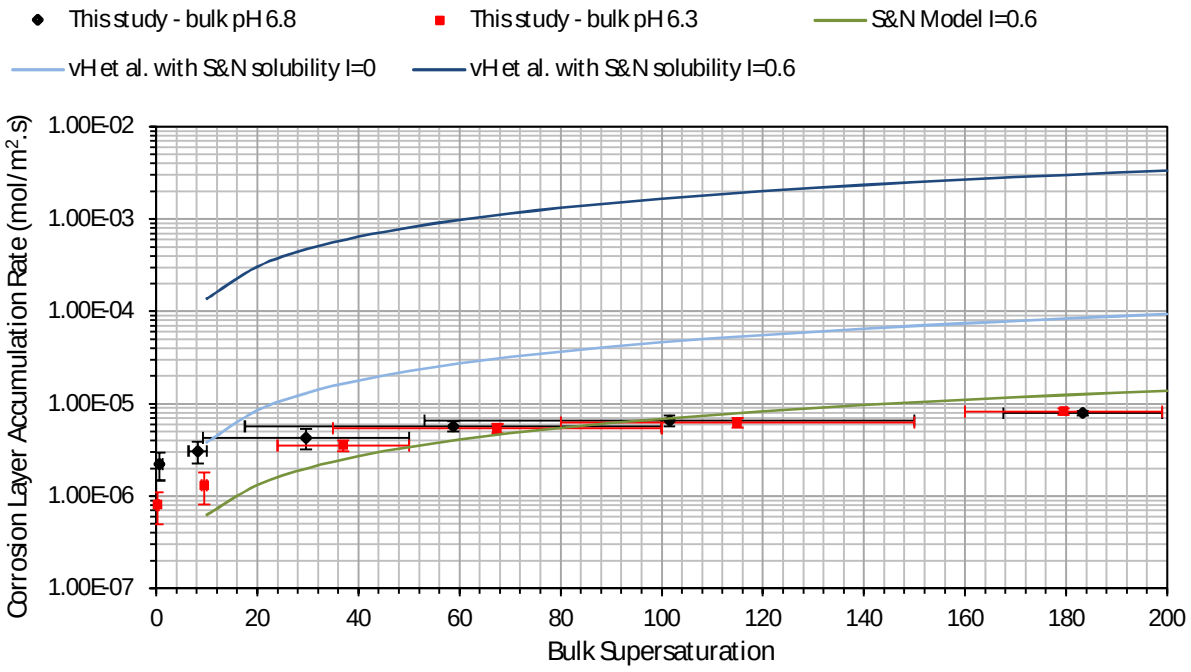

(a)

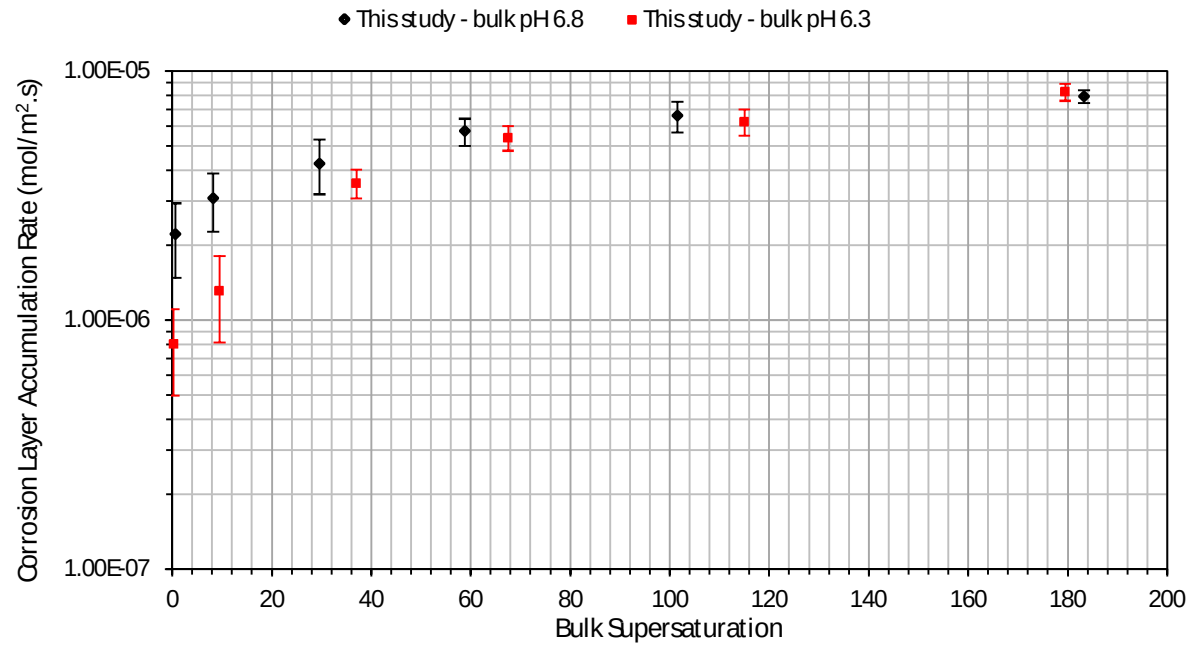

(b)

Figure 6: Measured CLARs for $FeCO_3$ for supersaturation levels from 0 to 200 at a temperature of 80℃ at pH 6.3 and 6.8 onto wet-ground X65 steel (a) in comparison to four models in literature and (b) plotted separately for clarity.

The reason behind this substantial difference in CLARs determined at pH 6.3 and pH 6.8 at low supersaturation can be attributed to the disparity in surface supersaturation at each pH. Particularly in static or low flow rate systems, the surface conditions can be

vastly different to those of the bulk solution[13]. Despite the tests at pH 6.3 and 6.8 having the same initial bulk supersaturation, the extent to which the solubility is locally exceeded at the surface of the corroding steel is likely to be significantly different, particularly at low levels of bulk supersaturation. Based on previous research under identical conditions, the initial corrosion rate of the X65 steel surface at pH 6.3 and 6.8 is very similar (peak corrosion rates of ~1.2 vs 1.0 mm/year for pH 6.3 and 6.8, respectively). This suggests that the surface flux of Fe^{2+} and consequently, the concentration of Fe^{2+} at the steel surface are very similar at each pH. However, at pH 6.8, approximately one order of magnitude less Fe^{2+} ions are required to obtain saturation of the bulk solution with respect to $FeCO_3$ compared to pH 6.3 due to the difference in bulk CO_3^{2-} concentration between the two systems. This essentially means that for a low bulk supersaturation, the initial supersaturation at the surface of a corroding steel surface would be significantly greater in a pH 6.8 solution compared to a pH 6.3 solution. This results in substantially faster surface deposition being observed at high pH, particularly at lower levels of bulk saturation, implying that the surface condition is dominating the CLAR process at low supersaturation, agreeing with the observations of Sun and Nesic[3].

As the bulk supersaturation increases, the dominance of $FeCO_3$ formation shifts from being significantly influenced by the corrosion process, to being controlled more by bulk supersaturation (as the percentage difference between the bulk and surface supersaturation decreases for each set of conditions). Here there is a convergence of the two CLARs at pH 6.3 and 6.8 where the bulk condition appears to have the overriding effect of controlling the kinetics. The results here reflect the fact that the surface concentration of species has a significant effect on the CLAR at low bulk supersaturation (in this instance, below a bulk supersaturation of ~60), and that accurate prediction of the kinetics of formation need to consider local saturation values if saturation level in the bulk solution is low. Figure 6(b) shows the deviation between the two CLARs more clearly, particularly at lower values of saturation.

3.3 Generation of protective film with reproducible mass

Experiments were conducted in order to grow a reproducible, highly protective $FeCO_3$ film which could then be exposed to conditions identical to those in the previous section. This enabled determination of the difference in CLAR for that onto a corroding wet-ground steel compared to a fully developed, protective corrosion product.

Figure 7 shows the corrosion rate response of X65 steel when exposed to 3.5 wt.% NaCl at pH 6.8 and 80°C, along with the Tafel response after 2 hours and 20 h. In Figure 7(a), the growth of $FeCO_3$ crystals suppresses the corrosion rate from ~1 mm/ year to below 0.05 mm/ year, significantly limiting the flux of Fe^{2+} from the steel surface. Figure 7(b) shows that this suppression of corrosion is achieved by reducing the kinetics of both the anodic and cathodic reaction. Average values for anodic and cathodic Tafel slopes (β_a and β_c) after corrosion product formation were determined to be 60±5 mV/ decade and 123±6 mV/ decade (producing a Stern-Geary coefficient of approximately 17.5±1.3, as shown in Table 3 along with the OCP and i_{corr} values), agreeing well with the theoretical values reported by Nesic et al.[19] at a temperature of 80°C. The average Tafel slopes values were used in conjunction with Equations (5) and (6) to express the transient charge-transfer resistance values measured using the Linear Polarisation Resistance technique as corrosion rates in mm/ year.

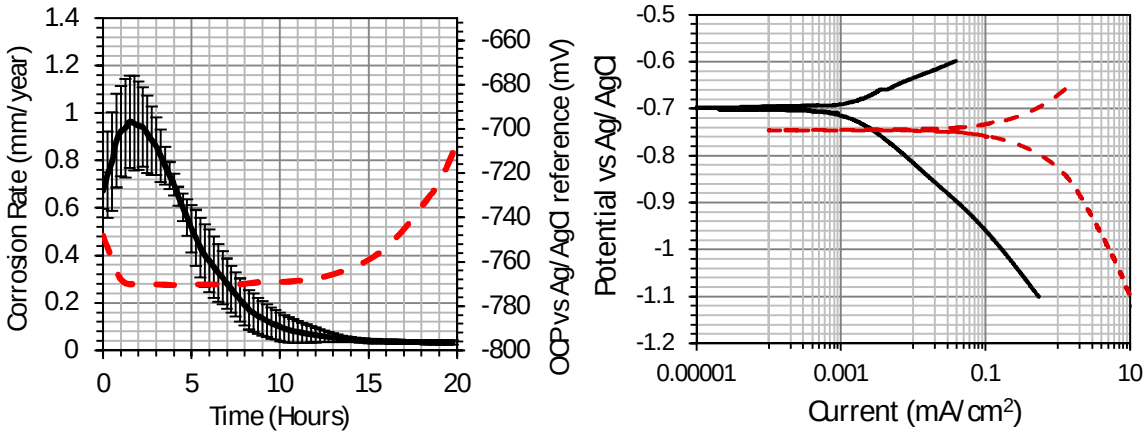

Figure 7: (a) Corrosion rate (black solid line) and OCP (red dashed line) vs time and (b) Tafel polarisation after 2 hours (red dashed line) and 20 h (black solid line) for X65 carbon steel exposed to 3.5 wt.% NaCl at pH 6.8 and 80°C

Table 3: Data extracted from Tafel measurements after $FeCO_3$ film formation

β_a (mV/ decade)	β_c (mV/ decade)	Stern-Geary coefficient (B)	OCP (mV)	I_{corr} (mA/ cm²)
60±5	123±6	17.5±1.3	-0.69	0.0025

Figure 8(a) shows and SEM image of the X65 steel surface at the end of the experiment shown in Figure 7(a) and indicates that in excess of 95% of the surface is covered by

$FeCO_3$ crystals, while the diffraction pattern in Figure 8(b) confirms the crystallographic structure of the corrosion product. Figure 9 indicates that the layer has a reproducible mass after multiple experiments, which was important given that additional CLAR experiments were conducted directly onto these established layers, and a high level of accuracy was required.

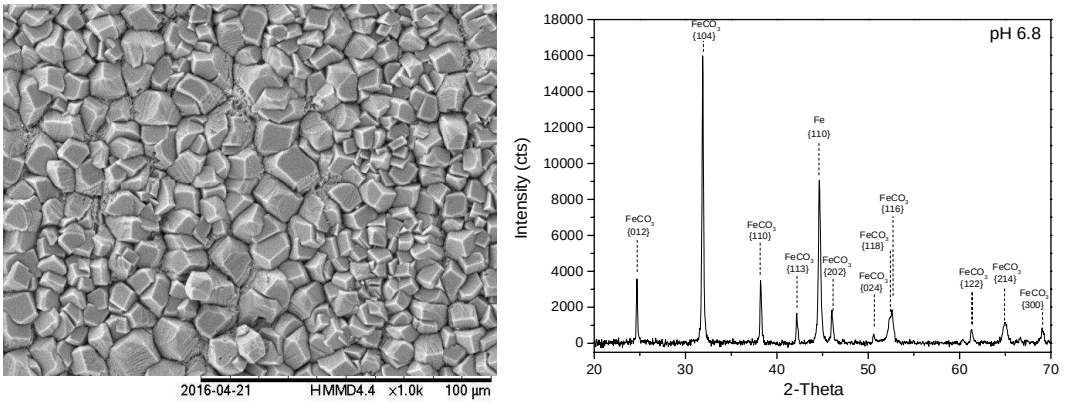

(a) **(b)**

Figure 8: (a) SEM image of $FeCO_3$ film formed on X65 steel after 20 h of immersion in 3.5 wt.% NaCl brine at 80°C; (b) XRD pattern from steel surface after immersion

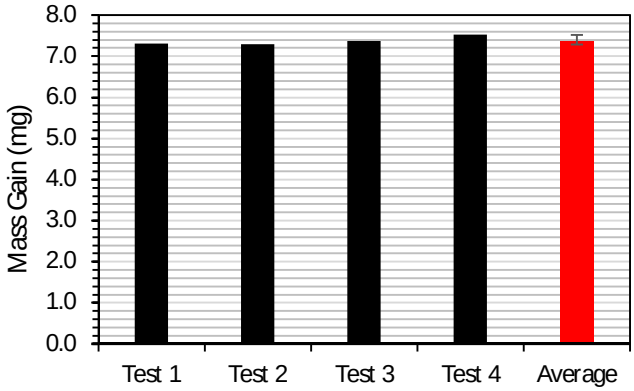

Figure 9: Mass of $FeCO_3$ layer on X65 steel after 20h; CO_2-saturated 3.5 wt.% NaCl solution and 80°C and pH 6.8

3.4 CLAR onto established $FeCO_3$ films

Figure 10 shows the CLARs onto the wet-ground steel surfaces compared to growth onto $FeCO_3$ filmed steels as a function of supersaturation. CLAR tests were conducted under the exact same conditions at pH 6.8 and 80°C for a period of 2 hours. At low S, the CLAR onto the established $FeCO_3$ film is far less favourable due to the lower surface supersaturation and the diminished Fe^{2+} production from the steel surface. These

observations are in agreement with Sun and Nesic[3] who stated that at low supersaturation, the CLAR is strongly affected by the corrosion rate of the steel surface. Although the same bulk supersaturation values can be obtained in each scenario at different levels of pH, for a corroding steel surface, the supersaturation at the steel surface will be dramatically higher for the higher pH system. This difference is likely to be intensified as pH increases if the corrosion rate of the steel surface remains similar (for the reasons stated previously).

At high bulk supersaturation, the influence of the corrosion process at the carbon steel surface has much less effect on the overall CLAR. This is perhaps at least partly attributed to the fact that rapid $FeCO_3$ deposition onto the corroding surface rapidly supresses the corrosion rate, limiting this effect. As stated by Sun and Nesic[3], the influence of the local supersaturation effect is more likely to manifest itself at low bulk supersaturation and low temperature.

It is worth comparing the results reported here to those obtained by Sun and Nesic[3] based on their experiments performed on stainless steel. Their results indicated that there is a contribution to CLAR from both the bulk solution and from the corroding surface by comparing the CLAR onto both stainless steel and a corroding carbon steel in the same environment. However, there is a distinct difference between deposition onto non-corroding stainless steel and the continued formation onto a well-established, highly protective $FeCO_3$ film on carbon steel which is considered here. Through observation of micrographs, Sun and Nesic[3] reported that at a supersaturation of 60 at 80^{o}C, there is almost no corrosion product accumulation onto stainless steel, whereas a high accumulation rate is recorded onto $FeCO_3$ at a similar supersaturation in this study.

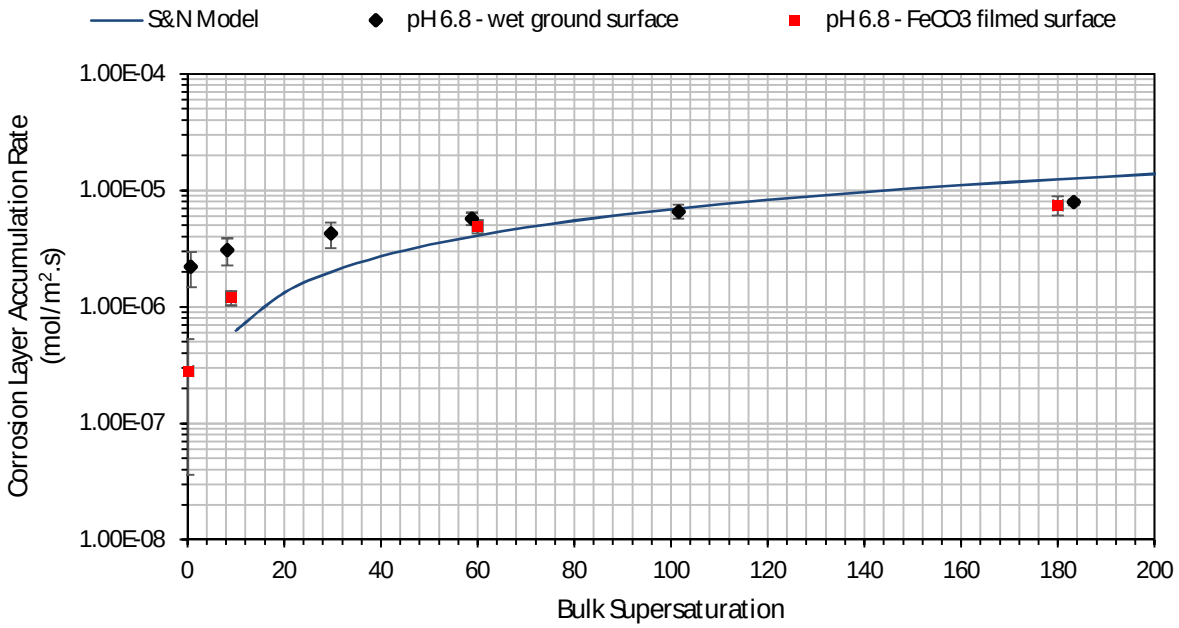

Figure 10: Predicted CLARs for $FeCO_3$ for bulk saturation ratios from 0 to 200 at a temperature of 80°C from the Sun and Nesic model compared to measured data obtained from the weight gain method onto wet-ground corroding carbon steel and an established $FeCO_3$ layer at pH 6.8.

Figure 11 shows an SEM image of the $FeCO_3$ layer after subsequent exposure to a CO_2-saturated 3.5 wt.% NaCl brine at pH 6.8 and 80°C with an initial bulk supersaturation of 200. Comparing this image with Figure 8(a) it is apparent that the film has continued to grow and there are clear areas where secondary nucleation has occurred on top of the pre-formed $FeCO_3$ crystals. The formation of these new $FeCO_3$ crystals begins with heterogeneous surface nucleation where part of the free-energy cost necessary for creating a new interface surrounding the nucleating phase has already been paid. This is known to be affected by the periodicity of the substrate and the nuclei; where a close registry between the two lattices such as epitaxial relationship increase nucleation rate[20]. This explains the discrepancy observed between the results of Sun and Nesic[3] using stainless steel where the small number of $FeCO_3$ crystals reflects the poor match offered by the substrate and the $FeCO_3$ secondary nucleation on preformed $FeCO_3$ film. The work highlights the impact of the substrate physico-chemical properties on the nucleation rate of $FeCO_3$ and demonstrates that continued accumulation onto an existing $FeCO_3$ is more favourable compared to stainless steel, which is worthy of consideration.

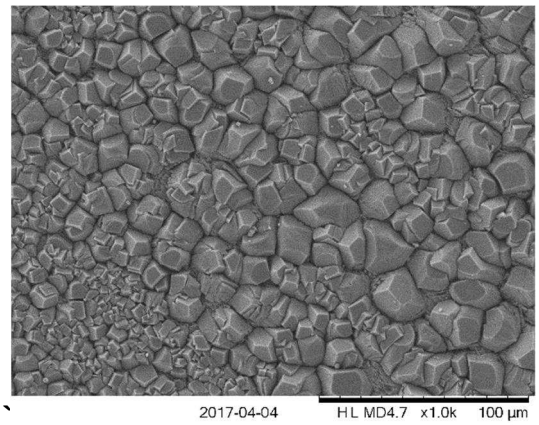

Figure 11: SEM image of $FeCO_3$ crystals precipitated on to an already existing $FeCO_3$ filmed X65 steel surface. Initial film was grown for 20 h in a CO_2-saturated 3.5 wt.% NaCl brine at 80°C and pH 6.8, then exposed to the same conditions at an SR of 200 for 2 hours.

The values in Figure 12 show the percentage difference between CLAR onto $FeCO_3$ and that onto wet-ground corroding steel as a function of initial bulk supersaturation values of 0, 10, 100 and 200. These were determined using Equation (11):

$$\%\ CLAR = \frac{CLAR_{wet-ground} - CLAR_{FeCO3}}{CLAR_{wet-ground}} \times 100 \quad (11)$$

where % CLAR is the percentage difference between deposition onto the $FeCO_3$ steel and that onto wet-ground corroding steel, $CLAR_{FeCO3}$ is the deposition onto the established $FeCO_3$ film and $CLAR_{wet\text{-}ground}$ is the deposition rate onto a corroding wet-ground steel surface, each for the same initial bulk supersaturation.

In the sense of the transient response of $FeCO_3$ deposition onto a corroding steel surface, this percentage essentially reflects the difference between the initial deposition rate onto the steel (influenced by the surface flux and bulk supersaturation) from that of the deposition rate once a protective film is established (influenced predominantly by the bulk conditions). The percentage can also be thought of as an indication as to the importance or significance of the corrosion process (or Fe^{2+} flux from the surface) on the CLAR in the early stages of growth. Essentially, the higher the percentage, the greater the contribution and importance of corrosion and local chemistry towards the CLAR during the initial film growth process.

According to Figure 12, at low supersaturation there is the greatest percentage difference between the two CLARs for the same bulk concentration. This is expected given the CLAR

in the presence of a protective film is extremely low when the bulk supersaturation is close to 0. As the bulk supersaturation increases, the difference in rates diminishes, until ultimately at high bulk supersaturation, there is little difference between the two rates. Under these conditions, the fact that a protective film establishes itself on the steel surface has little effect on the overall CLAR under these conditions. Unfortunately, a large experimental error is associated with these calculations given the fact that cumulative errors from multiple techniques need to be taken into account.

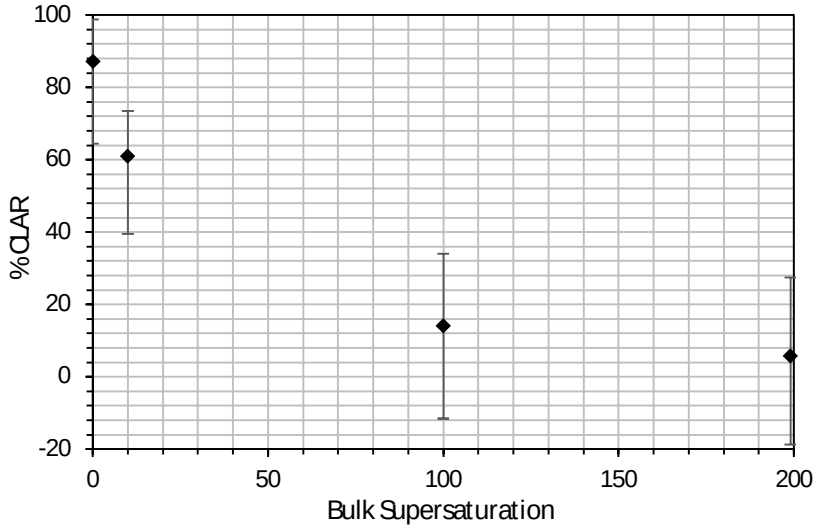

Figure 12: Percentage difference between CLARs onto wet-ground steel compared to steel pre-filmed with $FeCO_3$.

Overall, the results show that for low bulk supersaturation values, an increase in bulk pH magnifies the contribution of surface conditions to the CLAR, there is significant contribution to corrosion product formation from the corrosion process, and this dominates the process. In terms of modelling the time dependency of the CLAR, one model considering purely the bulk conditions is not sufficient. A universal expression linking surface supersaturation to deposition rate across a variety of conditions is required. Such a model also needs to consider the occupation of active sites on the steel surface and the corresponding suppression of Fe^{2+} flux from the steel surface with time.

4. Conclusion

In this paper, the corrosion layer accumulation rate (CLAR) of $FeCO_3$ is characterised on both an actively corroding carbon steel surface (at pH 6.3 and 6.8 at 80°C) and onto a

well-established, highly protective, $FeCO_3$-filmed steel surface (at pH 6.8 and 80°C). The purpose of the work was to establish how the $FeCO_3$ kinetics shift as the surface transitions from the early stages of corrosion (actively corroding) to the latter stages whereby there is protective film formation. The following conclusions from this study can be made:

- A distinction needs to be made between precipitation rate (i.e. precipitation in the entire system) and CLAR (i.e. deposition rate onto the steel surface). In some instances, significant precipitation of $FeCO_3$ can occur within the bulk solution, as well as accumulation onto the steel surface. This can lead to over-estimation of surface deposition rate (or CLAR) when using the Fe^{2+} measurements of the bulk solution to determine the rate of $FeCO_3$ formation on substrates.
- Based on the previous point, the use of corrosion layer mass gain measurements provides a better assessment of surface deposition rates of $FeCO_3$. Consequently, the CLAR model developed by Sun and Nesic is arguably the most reliable model developed to date under uninhibited conditions.
- CLARs at pH 6.3 and 6.8 were compared as a function of bulk supersaturation for actively corroding carbon steel samples. Although good agreement was observed between CLARs for both conditions at high bulk supersaturation (> ~ 60) (as well as with the model of Sun and Nesic), there was a disparity at low supersaturation where the higher bulk pH system produced higher deposition rates for the same bulk supersaturation values. This behaviour was attributed to the difference in surface supersaturation at each pH, despite the solutions having the same bulk supersaturation.
- For low bulk supersaturation values, an increase in bulk pH magnifies the contribution of surface conditions to the CLAR, resulting in significant contribution to deposition from the corrosion process.
- A comparison was made between CLARs recorded onto a corroding steel at pH 6.8 versus a steel surface pre-filmed with $FeCO_3$ under the same conditions. Examining the CLAR onto each surface as a function of bulk supersaturation revealed the importance of local supersaturation on the deposition rate at lower values of bulk supersaturation. The corroding surface was subjected to higher CLARs and compared to the pre-filmed sample. The difference between the two

rates was negligible at high bulk supersaturation, but increased significantly as bulk supersaturation was reduced.

- Once a protective $FeCO_3$ layer develops, the deposition kinetics can shift significantly if the supersaturation of the bulk solution is low. This transient response needs to be accounted for in CLAR models.

5. References

[1] R. Barker, Y. Hua, A. Neville, Internal corrosion of carbon steel pipelines for dense-phase CO_2 transport in carbon capture and storage (CCS)–a review, International Materials Reviews, 62 (2017) 1-31.

[2] D. Burkle, R. De Motte, W. Taleb, A. Kleppe, T. Comyn, S. Vargas, A. Neville, R. Barker, In situ SR-XRD study of $FeCO_3$ precipitation kinetics onto carbon steel in CO_2-containing environments: The influence of brine pH, Electrochimica Acta, 255 (2017) 127-144.

[3] W. Sun, S. Nešic, Kinetics of corrosion layer formation: Part 1-Iron carbonate layers in carbon dioxide corrosion, Corrosion, 64 (2008) 334-346.

[4] A. Dugstad, Fundamental aspects of CO_2 metal loss corrosion - Part 1: Mechanism, CORROSION 2006, San Diego, CA: NACE International Conference, 2006.

[5] F. Pessu, R. Barker, A. Neville, The influence of pH on localized corrosion behavior of X65 carbon steel in CO_2-saturated brines, Corrosion, 71 (2015) 1452-1466.

[6] D. Burkle, R. De Motte, W. Taleb, A. Kleppe, T. Comyn, S. Vargas, A. Neville, R. Barker, Development of an electrochemically integrated SR-GIXRD flow cell to study $FeCO_3$ formation kinetics, Review of Scientific Instruments, 87 (2016) 105125.

[7] S. Ieamsupapong, B. Brown, M. Singer, S. Nesic, Effect of solution pH on corrosion product layer formation in a controlled water chemistry system, CORROSION 2017, New Orleans, LA: NACE International Conference, 2017.

[8] E. Van Hunnik, E. Hendriksen, B.F. Pots, The formation of protective $FeCO_3$ corrosion product layers in CO_2 corrosion, CORROSION 96, Denver, CO: NACE International Conference, 1996.

[9] J. Greenberg, M. Tomson, Precipitation and dissolution kinetics and equilibria of aqueous ferrous carbonate vs temperature, Applied Geochemistry, 7 (1992) 185-190.

[10] J. Greenberg, High temperature kinetics of precipitation and dissolution of ferrous-carbonate, Masters Thesis, Rice University 1987.

[11] M. Johnson, M. Tomson, Ferrous carbonate precipitation kinetics and its impact CO_2 corrosion, CORROSION 91, NACE, Houston, TX: NACE International Conference, 1991.

[12] M. Nordsveen, S. Nešic, R. Nyborg, A. Stangeland, A mechanistic model for carbon dioxide corrosion of mild steel in the presence of protective iron carbonate films-Part 1: Theory and verification, Corrosion, 59 (2003) 443-456.

[13] S. Nešic, M. Nordsveen, R. Nyborg, A. Stangeland, A mechanistic model for carbon dioxide corrosion of mild steel in the presence of protective iron carbonate films—Part 2: A numerical experiment, Corrosion, 59 (2003) 489-497.

[14] J. Han, B.N. Brown, D. Young, S. Nešić, Mesh-capped probe design for direct pH measurements at an actively corroding metal surface, Journal of applied electrochemistry, 40 (2010) 683-690.

[15] R. De Motte, R. Barker, D. Burkle, S. Vargas, A. Neville, The early stages of $FeCO_3$ scale formation kinetics in CO_2 corrosion, Materials Chemistry and Physics, 216 (2018) 102-111.

[16] S. Guo, L. Xu, L. Zhang, W. Chang, M. Lu, Corrosion of alloy steels containing 2% chromium in CO_2 environments, Corrosion Science, 63 (2012) 246-258.

[17] R. Barker, D. Burkle, T. Charpentier, H. Thompson, A. Neville, A review of iron carbonate ($FeCO_3$) formation in the oil and gas industry, Submitted to Corrosion Science, (2018).

[18] E. Gulbrandsen, Acetic acid and carbon dioxide corrosion of carbon steel covered with iron carbonate, CORROSION 2007, NACE International, Nashville, TN: NACE International Conference, 2007.

[19] S. Nešić, J. Postlethwaite, S. Olsen, An electrochemical model for prediction of corrosion of mild steel in aqueous carbon dioxide solutions, Corrosion, 52 (1996) 280-294.

[20] D. Turnbull, B. Vonnegut, Nucleation catalysis, Industrial & Engineering Chemistry, 44 (1952) 1292-1298.